JACS
JOURNAL OF THE AMERICAN CHEMICAL SOCIETY

Communication

pubs.acs.org/JACS

Efficient Delivery of Quantum Dots into the Cytosol of Cells Using Cell-Penetrating Poly(disulfide)s

Emmanuel Derivery,[*,§,‡] Eline Bartolami,[†,‡] Stefan Matile,[*,†] and Marcos Gonzalez-Gaitan[*,†]

[†]School of Chemistry and Biochemistry, National Centre of Competence in Research (NCCR) Chemical Biology, University of Geneva, Quai Ernest Ansermet 30, CH-1211 Geneva, Switzerland

[§]MRC Laboratory of Molecular Biology, Francis Crick Avenue, Cambridge Biomedical Campus, Cambridge CB2 0QH, United Kingdom

Supporting Information

ABSTRACT: Quantum dots (QDs) are extremely bright, photostable, nanometer particles broadly used to investigate single molecule dynamics *in vitro*. However, the use of QDs *in vivo* to investigate single molecule dynamics is impaired by the absence of an efficient way to chemically deliver them into the cytosol of cells. Indeed, current methods (using cell-penetrating peptides for instance) provide very low yields: QDs stay at the plasma membrane or are trapped in endosomes. Here, we introduce a technology based on cell-penetrating poly(disulfide)s that solves this problem: we deliver about 70 QDs per cell, and 90% appear to freely diffuse in the cytosol. Furthermore, these QDs can be functionalized, carrying GFP or anti-GFP nanobodies for instance. Our technology thus paves the way toward single molecule imaging in cells and living animals, allowing to probe biophysical properties of the cytosol.

Understanding how tissue and cellular behavior emerges from single molecule dynamics is a major endeavor of modern cell biology. This faces a unique challenge because single molecule dynamics occurs at very short time scales (milliseconds), whereas cell and tissue dynamics occur at time scales of minutes or even hours. Meeting this challenge requires the ability to label single proteins in cells with bright yet photostable dyes, in order to maintain good localization precision over hours despite the small exposure time. In this context, quantum dots (QDs) are of particular interest because these nanometer-scaled particles are bright, photostable and amenable to functionalization.[1]

Though numerous studies have elegantly used QDs to investigate transmembrane protein dynamics at the plasma membrane,[2,3] their use to investigate single molecule dynamics in the cytoplasm has suffered from the lack of an efficient cytosolic delivery technique. Until today, physical methods such as microinjection,[4] electroporation[5] or osmotic shock[6] remain the most efficient way to introduce QDs in the cytosol. Chemical approaches to reliably deliver QDs in the cytosol do not exist, despite multiple efforts focusing mostly on cell-penetrating peptides (CPPs).[7−12] Here, we show that cell-penetrating poly(disulfide)s[13] (CPDs, Figure 1A) can meet this challenge. CPDs have recently been introduced to overcome the two main limitations of CPPs: endosomal capture and toxicity.[9,12] CPDs achieve this through thiol-mediated uptake[14,15] and reductive depolymerization upon arrival in the cytosol, respectively.

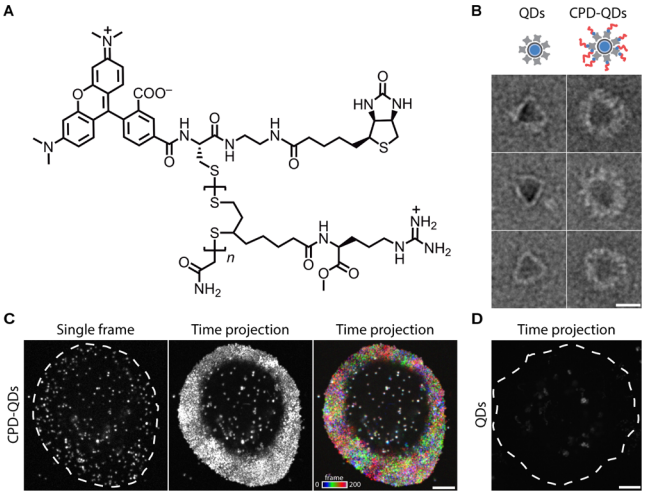

Figure 1. (A) Structure of the CPDs used in this study (n = 49). (B) TEM micrographs of streptavidin-functionalized QDs without (left) or after incubation with CPDs (right; CPD/QD = 62:1, 1 h, 4 °C), followed by negative staining. (C) Left panel: Live S2 cells incubated for 1 h with 3.33 nM CPD-QD complexes (62:1). Single confocal plane, n = 197 QDs. Middle panel: Time projection of a movie of the cell shown in the left panel. Right panel: Same time projection, color-coded according to frame number. (D) Cell incubated for 1 h with 6.66 nM QDs. Time projection as in C. Dash: cell outlines; scale bars: 10 nm (B), 5 μm (C,D).

In this study, we bound biotinylated CPDs[16,17] to streptavidin-coated QDs (CdSe core with ZnS shell, providing 20−40 biotin binding sites according to the manufacturer). We also replaced the original CF dye[16] by the red TAMRA (Figure 1A), leaving the green imaging channel free for further QD functionalization and colocalization experiments (see below). To optimize the uptake efficiency, long CPDs with n = 49 were prepared (M_w = 21.3 kDa, PDI = 1.09; see Supporting Information for full synthesis details and characterization, Schemes S1−S5 and Figures S1−S9). Upon incubation with an excess of these CPDs, QD diameter increased from d = 14.2 ±

Received: March 24, 2017
Published: July 25, 2017

DOI: 10.1021/jacs.7b02952
J. Am. Chem. Soc. 2017, 139, 10172−10175

0.8 to d = 18.3 ± 0.8 nm (transmission electron microscopy, n = 10, Figure 1B). The surface coverage of QDs with CPDs is complete and uniform (Figure 1B).

At low nanomolar concentrations, CPD-QD complexes were efficiently delivered into cultured *Drosophila* S2 cells (Figures 1C, S10). CPD-mediated QD delivery was not restricted to a particular cell state or phase because QDs were found in all cells under these conditions (n = 69 cells). On average, the number of internalized QDs per cell was 66 ± 9 (mean ± SEM, n = 36 cells). Most internalized QDs were very motile and excluded from the nucleus (Figures 1C, S10, Movie S1).

Dose response experiments suggested that a 2-fold molar excess of CPD over QDs was sufficient for efficient delivery (Figure S11), implying that only few CPD molecules are required per QD, if we assume homogeneous streptavidin-functionalization of the QD population. In addition, neither QDs by themselves (Figure 1D), QDs incubated with biotin-free CPDs (Figure S12), nor QDs incubated with biotinylated CPDs in the presence of excess biotin (Figure S12) did efficiently enter into cells, but rather remained trapped in endosomal compartments. This suggests that cytosolic delivery requires specific interactions with CPDs, at least for streptavidin-coated QDs.

We then checked that QDs were indeed delivered into the cytosol using three independent methods (see below): (i) delivered QDs have a diffusive motion with a diffusion coefficient too high for endosomes (mean square displacement (MSD) analysis), (ii) QDs have low colocalization with endosomal markers and (iii) most QDs are found beyond the plasma membrane imaged by TIRFM (total internal reflection fluorescence microscopy).

We first characterized the motion of the QDs delivered into cells. An object of the size of a QD (~15 nm in diameter) moving freely in the cytosol would undergo Brownian motion with a fast diffusion coefficient, but would not perform long-range, processive, directed motility mediated by molecular motors.[6] On the other hand, endosomes (in which QDs could be trapped) are larger objects and therefore move with a lower diffusion coefficient; however, when engaging microtubule tracks through molecular motors, they show faster, processive, directed motility.[18] We automatically tracked the motion of thousands of delivered QDs and performed an MSD analysis (see Supporting Information for details). We observed three types of behavior: (i) short-range motion ("diffusive events"; Figure 2A, 87% of n = 10 127 tracks in N = 8 cells), (ii) long-range motility ("processive events"; Figure 2C; only four tracks found in our extended N = 27 cells data set) and (iii) immobility.

Short-range motility tracks correspond to subdiffusive events because their MSD as a function of delay time is described by a power law function[19] (R^2 = 0.99; α = 0.648 ± 0.012, D = 0.111 ± 0.001 $\mu m^2/s$, Figure 2B). Importantly, the diffusion coefficient of these QDs is 2 orders of magnitude higher than that reported for endosomes,[18] but in the range of QDs delivered to the cytosol by electroporation[5] or osmotic shock.[6] On the other hand, the four "long-range motility" tracks correspond to events of processive motility (Figure 2C) as their MSD curve is described by a quadratic function (R^2 = 0.9999, Figure 2D). This behavior is reminiscent of endosome motility driven by molecular motors. Consistently, the mean velocity, v = 0.366 ± 0.002 $\mu m/s$, is in the range of motor-driven endosome motility in cells.[18,20] Altogether, this suggests that the vast majority of CPD-delivered QDs display motion

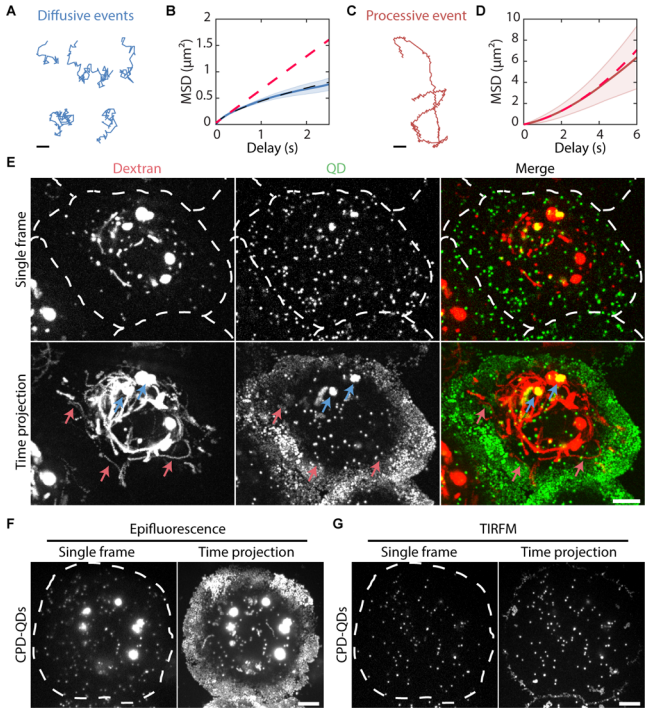

Figure 2. (A) Examples of short-range motion tracks of CPD-delivered QDs. (B) Quantitative analysis of short-range tracks. Blue line (solid): Weighted mean square displacement (MSD) as a function of delay time of short-range tracks (n = 8856 tracks, lighter area: SEM). Dashed black line: power law fit reflecting subdiffusion (R^2 = 0.99). Dashed red line: linear fit of the first five points of the curve (R^2 = 0.99). (C) Example of a long-range motility track (<0.1% of total tracks). (D) Quantitative analysis of long-range tracks. Solid red line: weighted MSD as a function of delay time of long-range motility tracks (n = 4 tracks, lighter area: SEM). Dashed red line: parabolic fit (reflecting directed motility combined with diffusion, R^2 = 0.9999). (E) Snapshot (top) and time projection (bottom) of S2 cells incubated with CPD-QDs (green) and fluorescently labeled dextran (red). (F, G) Snapshot (left) and time projection (right) of CPD-QDs imaged by epifluorescence, which illuminates the entire cells (F) and TIRF microscopy, which only illuminates the ventral plasma membrane (G). CPD/QD = 62:1, scale bars: 1 μm (A, C), 5 μm (E–G).

characteristics incompatible with endosome motility, but consistent with subdiffusive, Brownian motion in the cytosol.

Second, we studied the localization of CPD-delivered QDs with respect to endosomes using endosomal markers. We combined CPD-mediated QD uptake with a long chase of fluorescent dextran, which labels both early and late endosomal compartments (Figures 2E, S13, Movie S2). We found a low colocalization (10 ± 1%; N = 36 cells, see Supporting Information), confirming that most QDs are indeed not in endosomes. Analysis of dual color movies further confirmed our automated tracking analysis: QDs nearly never colocalize with dextran-positive endosomes, which moved processively (Figure 2E, S13; time projection, red arrows). In contrast, the few QDs that did colocalize with dextran were mostly immobile (Figure 2E, S13; blue arrows). These immobile QDs (~13% of the tracks in our automated analysis) may thus correspond to QDs trapped in large immobile compartments (and/or abortive endocytosis events, see below).

Third, we confirmed that most QDs are found deep in the cytosol using TIRFM. TIRFM images only the first 100 nm of the ventral plasma membrane and excludes deeper optical

DOI: 10.1021/jacs.7b02952
J. Am. Chem. Soc. 2017, 139, 10172–10175

planes within the cytoplasm, whereas epifluorescence illuminates the whole cell. Though a minority of QDs was immobile at the plasma membrane (appearing in both epifluorescence and TIRFM fields), most QDs are diffusive and appear in the epifluorescence field but not in the TIRF field (Figure 2F,G, Movie S3). This indicates that most of the QDs uptaken by the cell are deep into the cytosol and do not correspond to QDs bound to the plasma membrane. Importantly, we verified using four mammalian cell lines that the CPD-mediated cytosolic delivery of QDs is not restricted to insect cells (Figures S14–S15, Movie S4).

We then checked whether the remaining biotin-binding sites of QDs, which were not used for CPD binding, could be used to deliver proteins bound to the QDs. GFP-CPD-QDs were prepared by incubation of streptavidin-QDs with purified biotinylated GFP (3:1) then with CPDs (63:1, Figure 3A).

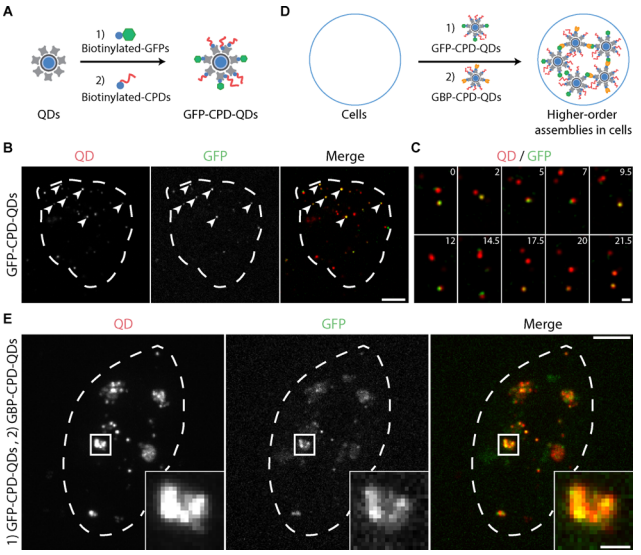

Figure 3. (A) Sequential functionalization of QDs with GFP or GFP-nanobodies and CPDs. (B) Single confocal plane of a live S2 cell incubated for 1 h with 6.8 nM GFP-CPD-QDs (3:63:1). Arrowheads: GFP-positive QDs. (C) Snapshots of a movie of the cell displayed in panel B. Note the continuous colocalization between QD and GFP signals. Occasional partial colocalization reflects the slow acquisition of the two channels compared to the fast diffusive motion of QDs. (D) Large cytosolic QD assemblies occur upon sequential delivery of GFP-CPD-QDs and GBP-CPD-QDs (GBP: Anti-GFP nanobody). (E) Image of live S2 cell incubated for 1 h with 6.66 nM GFP-CPD-QDs (3:63:1), followed by 6.66 nM GBP-CPD-QDs (11:61:1). Images correspond to maximum intensity z-projections. Note the cytosolic aggregates of QDs. Dash: cell outlines. Scale bars: 5 μm (1 μm in insets).

Upon incubation with cells, many internalized GFP-positive QDs were observed (Figures 3B,C, S16, S17). Their motility properties were similar to the delivered CPD-QDs (Figures 3C, S19A,B; $D = 0.103 \pm 0.001$ $\mu m^2/s$, 95% confidence interval, n = 7453 tracks in N = 7 cells). Delivery of CPD-QDs with biotinylated anti-GFP nanobodies[21] gave similar results (GBP: GFP binding peptide, $R^2 = 0.999$, $D = 0.131 \pm 0.001$ $\mu m^2/s$, $\alpha = 0.840 \pm 0.004$, 95% confidence interval, n = 4169 tracks in N = 3 cells for GBP-QDs; Figures 3D, S19C). Thus, functionalization of QDs with GFP or GBP did not affect their efficient cytosolic delivery by CPDs.

Sequential delivery of GFP-functionalized QDs followed by GBP-functionalized QDs caused the appearance of large aggregates of GFP-positive QDs in the cytosol (Figures 3E, S18). This suggests that GBP bound to the QD retains its GFP-binding properties in the cytosol. GFPs bound to the QDs also retain their fluorescence (Figures 3B–E and S16–S18). Therefore, CPDs allow the delivery of proteins in their native, functional state (Figure 3D).

The cytosolic delivery of particles and proteins is an area of intense investigation due to its potential applications: in clinics, it is expected to allow therapeutic antibodies to access cytosolic targets, whereas in life science research, it can be used to image and manipulate single molecules inside cultured cells or animals. In this context, the cytosolic delivery of functionalized QDs has emerged as one of the most persistent challenges. In this report, we demonstrate that biotinylated CPDs deliver streptavidin-coated QDs efficiently (about 70 per cell), and that most of these QDs (about 90%) reach the cytosol without being trapped in intracellular compartments or at the plasma membrane (Figures 1, 2). Because just a few CPD molecules are sufficient for QD delivery, some binding sites on the QDs remain free for further interfacing with other proteins (Figure 3). Those proteins stay functional upon delivery.

In this report, we determined unambiguously the cytosolic location of the CPD-delivered QDs. This was motivated by previous reports using CPPs, which showed that they do not reach the cytosol and remain trapped in endosomes.[1,7,8,11] Although CPP architecture is similar to the present CPD-QDs, they enter the endosome network by macropinocytosis; CPP-QD filled endosomes then move along microtubules toward the microtubule-organizing center, only to turn around and move outward into filopodia to be expelled by vesicle shedding.[11]

The efficient cytosolic delivery by CPDs originates from the combination of two independent uptake mechanisms involving counterion activators (as with CPPs), and dynamic covalent disulfide exchange with thiols on cell surfaces.[12] Accordingly, CPD uptake is insensitive to endocytosis inhibitors, weakly depending on temperature and strongly depending on thiol-mediated uptake inhibitors.[13,17] The fact that only few CPDs per QD are sufficient for delivery is in agreement with counterion-mediated direct translocation through nonleaky micellar defects. Their dynamic adjustment to the substrate and their ability to self-repair after translocation further contributes to low toxicity. Furthermore, destruction of CPDs upon entry into the cytosol ensures irreversibility and minimizes toxicity.[12,13] CPDs conjugated to other small fluorophores have indeed been confirmed to be much less toxic than CPPs.[13] Though extensive toxicity studies of CPD-QDs have not yet been carried out, the low toxicity of CPDs conferred by their intracellular degradation is characteristic of this delivery platform. Importantly, long-term toxicity, which is inherent to Cd release from QDs, is unrelated to the topic of this study.[1−8]

The delivery technology introduced here will offer a new avenue for biologists to address the biochemical and biophysical properties of proteins in intact cells, and also within animals. The high number of QDs delivered per cell and the efficiency of delivery across the cell population allows one to follow thousands of single molecules in thousands of cells, yielding precise statistics in time and space. This will be particularly useful for the study of intrinsically stochastic molecular machines, such as molecular motors, thereby generalizing to tissues or whole animals the very elegant approach recently described by the Kapitein lab using electroporation.[5b]

DOI: 10.1021/jacs.7b02952
J. Am. Chem. Soc. 2017, 139, 10172−10175

■ ASSOCIATED CONTENT

Supporting Information

The Supporting Information is available free of charge on the ACS Publications website at DOI: 10.1021/jacs.7b02952.

Movies as described in text (ZIP)
Detailed experimental procedures (PDF)

■ AUTHOR INFORMATION

Corresponding Authors

*marcos.gonzalez@unige.ch
*stefan.matile@unige.ch
*derivery@mrc-lmb.cam.ac.uk

ORCID

Emmanuel Derivery: 0000-0003-3927-5944
Stefan Matile: 0000-0002-8537-8349

Author Contributions

‡E.D. and E.B. contributed equally.

Notes

The authors declare no competing financial interest.

■ ACKNOWLEDGMENTS

We thank Nicolas Chiaruttini for help with EM, Paola Morelli for assistance with synthesis, the NMR, MS and bioimaging platforms for services, and the University of Geneva, the NCCR Chemical Biology and the Swiss NSF for financial support. M.G.-G. is further supported by the SystemsX (epiPhysX), ERC (Sara and Morphogen) and Polish-Swiss programs, S.M. by the NCCR Molecular Systems Engineering and E.D. by the Medical Research Council (file reference number MC_UP_1201/13) and HFSP (LTF and CDA).

■ REFERENCES

(1) Hildebrandt, N.; Spillmann, C. M.; Algar, W. R.; Pons, T.; Stewart, M. H.; Oh, E.; Susumu, K.; Díaz, S. B.; Delehanty, J. B.; Medintz, I. L. *Chem. Rev.* **2017**, *117*, 536−711.
(2) Bouzigues, C.; Morel, M.; Triller, A.; Dahan, M. *Proc. Natl. Acad. Sci. U. S. A.* **2007**, *104*, 11251−11256.
(3) Chung, I.; Akita, R.; Vandlen, R.; Toomre, D.; Schlessinger, J.; Mellman, I. *Nature* **2010**, *464*, 783−787.
(4) Damalakiene, L.; Karabanovas, V.; Bagdonas, S.; Valius, M.; Rotomskis, R. *Int. J. Nanomed.* **2013**, *8*, 555−568.
(5) (a) Hatakeyama, H.; Nakahata, Y.; Yarimizu, H.; Kanzaki, M. *Mol. Biol. Cell* **2017**, *28*, 173−181. (b) Katrukha, E. A.; Mikhaylova, M.; van Brakel, H. X.; van Bergen En Henegouwen, P. M.; Akhmanova, A.; Hoogenraad, C. C.; Kapitein, L. C. *Nat. Commun.* **2017**, *8*, 14772.
(6) Courty, S.; Luccardini, C.; Bellaiche, Y.; Cappello, G.; Dahan, M. *Nano Lett.* **2006**, *6*, 1491−1495.
(7) Breger, J.; Delehanty, J. B.; Medintz, I. L. *WIREs Nanomed. Nanobiotechnol.* **2015**, *7*, 131−151.
(8) Delehanty, J. B.; Bradburne, C. E.; Susumu, K.; Boeneman, K.; Mei, B. C.; Farrell, D.; Blanco-Canosa, J. B.; Dawson, P. E.; Mattoussi, H.; Medintz, I. L. *J. Am. Chem. Soc.* **2011**, *133*, 10482−10489.
(9) (a) McKinlay, C. J.; Waymouth, R. M.; Wender, P. A. *J. Am. Chem. Soc.* **2016**, *138*, 3510−3517. (b) Li, M.; Schlesiger, S.; Knauer, S. K.; Schmuck, C. *Angew. Chem., Int. Ed.* **2015**, *54*, 2941−2944. (c) Bechara, C.; Sagan, S. *FEBS Lett.* **2013**, *587*, 1693−1702. (d) Herce, H. D.; Garcia, A. E.; Cardoso, M. C. *J. Am. Chem. Soc.* **2014**, *136*, 17459−17467. (e) Rodríguez, J.; Mosquera, J.; Couceiro, J. R.; Nitschke, J. R.; Vázquez, M. E.; Mascareñas, J. L. *J. Am. Chem. Soc.* **2017**, *139*, 55−58. (f) Nakase, I.; Akita, H.; Kogure, K.; Gräslund, A.; Langel, Ü.; Harashima, H.; Futaki, S. *Acc. Chem. Res.* **2012**, *45*, 1132−1139.
(10) Jablonski, A. E.; Kawakami, T.; Ting, A. Y.; Payne, C. K. *J. Phys. Chem. Lett.* **2010**, *1*, 1312−1315.
(11) Ruan, G.; Agrawal, A.; Marcus, A. I.; Nie, S. *J. Am. Chem. Soc.* **2007**, *129*, 14759−14766.
(12) Gasparini, G.; Bang, E.-K.; Montenegro, J.; Matile, S. *Chem. Commun.* **2015**, *51*, 10389−10402.
(13) Gasparini, G.; Bang, E.-K.; Molinard, G.; Tulumello, D. V.; Ward, S.; Kelley, S. O.; Roux, A.; Sakai, N.; Matile, S. *J. Am. Chem. Soc.* **2014**, *136*, 6069−6074.
(14) Chuard, N.; Gasparini, G.; Moreau, D.; Lörcher, S.; Palivan, C.; Meier, W.; Sakai, N.; Matile, S. *Angew. Chem., Int. Ed.* **2017**, *56*, 2947−2950.
(15) (a) Aubry, S.; Burlina, F.; Dupont, E.; Delaroche, D.; Joliot, A.; Lavielle, S.; Chassaing, G.; Sagan, S. *FASEB J.* **2009**, *23*, 2956−2967. (b) Oupický, D.; Li, J. *Macromol. Biosci.* **2014**, *14*, 908−922.
(16) Gasparini, G.; Matile, S. *Chem. Commun.* **2015**, *51*, 17160−17162.
(17) Fu, J.; Yu, C.; Li, L.; Yao, S. Q. *J. Am. Chem. Soc.* **2015**, *137*, 12153−12160.
(18) Derivery, E.; Seum, C.; Daeden, A.; Loubéry, S.; Holtzer, L.; Jülicher, F.; Gonzalez-Gaitan, M. *Nature* **2015**, *528*, 280−285.
(19) Metzler, R.; Klafter, J. *Phys. Rep.* **2000**, *339*, 1−77.
(20) Soppina, V.; Verhey, K. J. *Mol. Biol. Cell* **2014**, *25*, 2161−2170.
(21) Rothbauer, U.; Zolghadr, K.; Muyldermans, S.; Schepers, A.; Cardoso, M. C.; Leonhardt, H. *Mol. Cell. Proteomics* **2008**, *7*, 282−289.

DOI: 10.1021/jacs.7b02952
J. Am. Chem. Soc. 2017, 139, 10172−10175